The influence of molecular rotation on the direct subsurface absorption of H_2 on Pd(111)

R. A. Olsen[a)]
Theoretische Chemie, Vrije Universiteit, De Boelelaan 1083, 1081 HV Amsterdam, The Netherlands

G. J. Kroes
Leiden Institute of Chemistry, Gorlaeus Laboratories, Postbus 9502, 2300 RA Leiden, The Netherlands

E. J. Baerends
Theoretische Chemie, Vrije Universiteit, De Boelelaan 1083, 1081 HV Amsterdam, The Netherlands

(Received 24 February 1998; accepted 29 April 1998)

Within the generalized gradient approximation (GGA) of density functional theory (DFT) we have calculated a three-dimensional (3D) potential energy surface (PES) including an angular degree of freedom for a H_2 molecule interacting with a Pd(111) surface. There is an entrance channel barrier ($\approx$0.09 eV) to both dissociative chemisorption and direct subsurface absorption, but after this barrier is crossed direct subsurface absorption can proceed almost without a barrier. 3D quantum mechanical wave packet calculations incorporating the rotation of H_2 in a plane perpendicular to the surface show a large part of the hydrogen going directly subsurface even at low incident kinetic energies. The wave packet calculations also show that in the low energy regime rotation inhibits direct subsurface absorption at low j_0 and promotes it at high j_0. © *1998 American Institute of Physics.* [S0021-9606(98)70230-2]

I. INTRODUCTION

A number of experimental[1–7] and theoretical[2,3,8–19] studies indicate the existence of a hydrogen absorption site between the first and second metal layer on the Pd(111) surface, a so-called subsurface site, being energetically more stable than the bulk site and almost as favorable as the chemisorption state on the surface. The study of Gdowski, Stulen, and Felter[6] further presents evidence that hydrogen reaches this site directly, i.e., without first equilibrating in the chemisorption well on the surface.

The term direct subsurface absorption will be used to describe the process of a hydrogen molecule dissociating and one or both of its atoms going directly into the subsurface sites without equilibrating in the chemisorption wells on the surface. This is in contrast to the process in which the hydrogen molecule dissociates, its atoms equilibrate in the chemisorption wells on the surface, and then one or both of the atoms reach the subsurface sites by thermally assisted diffusion.

A first attempt to model the direct process through quantum mechanical wave packet calculations on a two-dimensional (2D) PES was made in Ref. 14. The model character of the PES made it difficult to draw any conclusions on the possibility for direct subsurface absorption—the authors therefore suggested efforts to improve the PES. They also indicated the need to increase the dimensionality of the PES. In Ref. 18 a 2D PES based on DFT within the GGA was presented. This PES had a barrier of about 0.9 eV (relative to the bottom of the H_2 gas phase potential) to subsurface penetration and the quantum mechanical wave packet calculations showed no direct subsurface absorption for incident kinetic energies below 0.74 eV. Thus the study did not support direct subsurface absorption as seen in the experiments of Gdowski, Stulen, and Felter.[6] This was attributed to the fact that only two degrees of freedom were treated rather than the DFT GGA level of theory not being appropriate for modeling the H_2+Pd(111) system well—the DFT GGA results were in fact shown to compare favorably with experimental results.[18] In Ref. 19 a palladium surface degree of freedom was added to the PES. Even though the quantum mechanical wave packet calculations on this 3D PES did not find hydrogen going directly subsurface for incident kinetic energies below 0.4 eV, the results showed important qualitative and quantitative effects upon including palladium surface motion.

In Ref. 17 Munn and Clary used the model PES introduced in Ref. 14 to include an angular degree of freedom in the PES. With this 3D PES their quantum mechanical calculations showed a substantial part of the hydrogen going directly subsurface at low incident energies. The authors themselves pointed out that the results of their calculations might have somewhat limited physical meaning due to the PES only being parametrized for one value of the angle and not the full range of angles needed for the 3D PES, but their study nevertheless very clearly showed the importance of including an angular degree of freedom in the PES.

In this paper we present a 3D PES based on DFT within the GGA for H_2 interacting with a Pd(111) surface including an angular degree of freedom for the hydrogen molecule. The 3D PES is then used in quantum mechanical wave packet calculations to investigate the effect of molecular rotation on the direct subsurface absorption and we compare the results with the experimental results of Gdowski, Stulen,

[a)]Electronic mail: olsen@chem.vu.nl

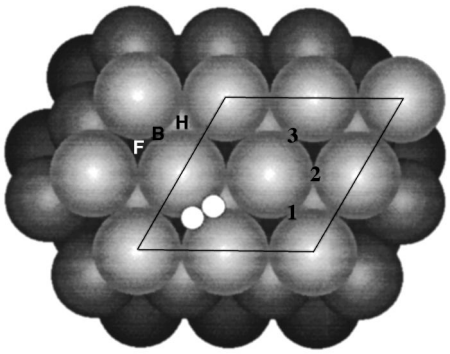

FIG. 1. The slab geometry used in the calculations of the PES. The 2×2 surface unit cell is marked by the solid lines. The two small white discs represent the hydrogen atoms. The bold letters F, B, and H designate the fcc, bridge, and hcp sites, respectively. Directly below the fcc site and between the first and second metal layers is the subsurface octahedral site. Directly below the hcp site and between the first and second metal layers is the subsurface tetrahedral site. The numbers 1, 2 and 3 label three bridge sites that differ only in the sense that the plane defined by the given bridge site and the neighboring fcc and hcp sites are rotated with respect to each other.

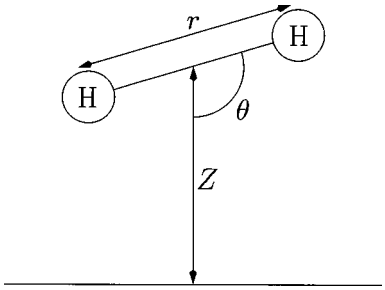

FIG. 2. The three degrees of freedom treated in this study are shown in the figure.

and Felter.[6] We also present the results of the effect of molecular rotation on the total reaction probability and compare this to experiments.

The paper is organized as follows. In Sec. II we present the new 3D PES, and the techniques used in the quantum mechanical wave packet calculations are described in Sec. III. In Sec. IV we present the results of the dynamical calculations, and our conclusions are given in Sec. V.

II. THE DFT PES CALCULATIONS

The BAND[20–22] program has been used to perform the electronic structure calculations. A detailed discussion of how the program performs for the H_2+Pd(111) system can be found in Ref. 18. There it was shown that the results were converged to within 0.1 eV of the DFT GGA limit for the H_2+Pd(111) system. We have used the same basis set and computational parameters for the present study. It has been shown that DFT at the GGA level compares favorably with experimentally known results for Pd bulk, PdH bulk, the H_2 molecule, and H_2 on Pd(111) (see Ref. 18 for details).

The calculations have been done on a three layer Pd(111) slab with hydrogen adsorbed/absorbed on one side of the slab within a 2×2 surface unit cell as illustrated in Fig. 1. The H_2 molecule's center of mass is kept above/below a bridge site and the hydrogen atoms move from the bridge site towards the two surface hollow sites, the fcc and hcp sites, and the subsurface sites directly beneath these. The molecule can rotate in a plane perpendicular to the surface, with the perpendicular plane going through the fcc and hcp sites. Thus the three degrees of freedom included in our PES are the hydrogen molecule's center of mass distance to the surface, Z (taken positive above the surface, negative below), the hydrogen molecule's bond distance, r, and a rotational angle, θ, all shown in Fig. 2. Geometries with $\theta>90$ degrees correspond to orientations which will allow one hydrogen atom to enter the subsurface region below a fcc site.

To be able to give a good description of the angular dependence of the PES six 2D PESs have been calculated with the angle fixed to 0, 30, 60, 90, 120, and 150 degrees, respectively. Each 2D PES is fitted to bicubic splines based on a set of about 70 points. The full 3D PES is expanded according to

$$V_{3D}(Z,r,\theta)=c_1'(Z,r)+c_2'(Z,r)\cos(2\theta)+c_3'(Z,r)\sin(2\theta)+c_4'(Z,r)\cos(4\theta)+c_5'(Z,r)\sin(4\theta)+c_6'(Z,r)\cos(6\theta). \quad (1)$$

The expansion coefficients $c_n'(Z,r)$ are found by inverting the set of linear equations one gets when inserting the values for the 2D PES's and their respective angles in Eq. (1).

In Fig. 3a the PES for $\theta=90$ degrees is shown. The PES describes a molecule approaching the bridge site with the molecular axis parallel to the surface plane and dissociating into the two surface hollow sites. The surface adsorption minimum with one atom close to the fcc site and the other close to the hcp site is stable by about 0.65 eV compared to the bottom of the H_2 gas phase potential. As discussed in Ref. 18 this agrees well with the experimental value for chemisorption. It also agrees well with the value of 0.69 eV given by Dong and Hafner.[23] As mentioned in Ref. 18, the PES has a small barrier in the entrance channel. The barrier is about 0.09 eV and since our calculations are only converged to within 0.1 eV we should take some care in putting too much trust in the existence of this barrier or the numerical value of its height. However, Dong, Kresse, and Hafner[24] also using DFT, but with a different method for solving the Kohn–Sham equations[25,26] and a different GGA, give a value of 71 meV for the barrier in the entrance channel when considering the same approach geometry. In a more recent study by Dong and Hafner[23] the value of 19 meV is given for the same barrier. This seems to indicate that there is a small barrier in the entrance channel for this approach geometry when studying the system at the GGA level within DFT. We will comment more on this in Sec. IV. Since in Fig. 3a the molecular axis is kept parallel to the surface both the hydrogen atoms are moved subsurface when the Z coordinate takes negative values. For the atom entering the subsurface region below the fcc site this causes no problem—it approaches a favorable absorption site, the octahedral subsurface site, which geometrically resembles the bulk octahedral site the hydrogen is known to occupy in bulk PdH.[27–30] But the atom entering the subsurface region below the hcp site comes too close to the Pd atom in the second metal layer directly beneath the hcp site—the tetrahedral subsurface site is not a

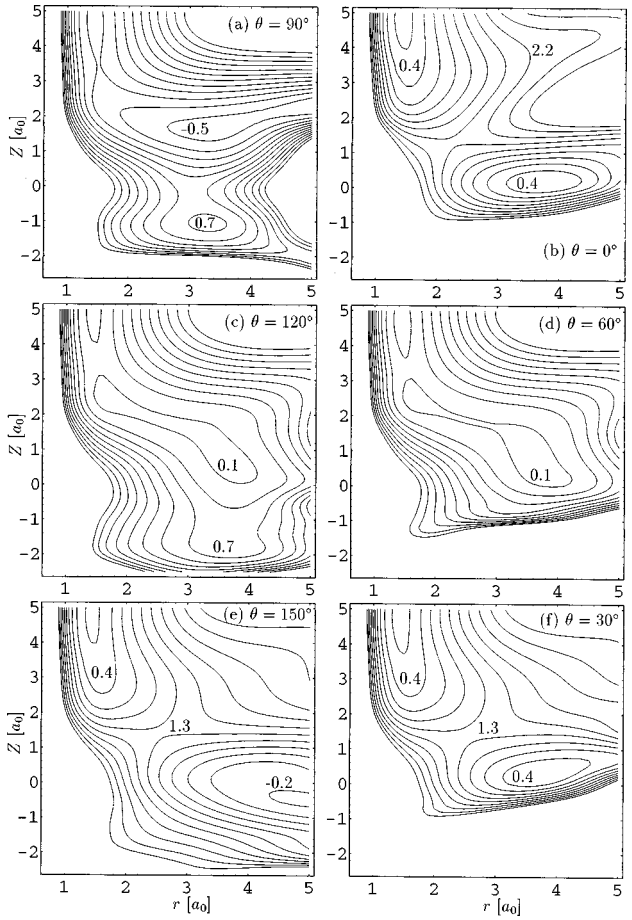

FIG. 3. The figures show contour plots of the six 2D PES's used to build up the 3D PES. The numbers within the contour plots are in eV and give the value of the contour line that lies closest by. In (e) and (f) the number 1.3 pertains to the two closest contour lines. The energies are given relative to the bottom of the H_2 gas phase potential. In all the six contour plots the first contour line near the bottom of the H_2 gas phase potential is 0.1 eV, and the contour spacing is 0.3 eV.

stable absorption site. Thus, as seen from Fig. 3a, the subsurface minimum is not stable with respect to the bottom of the H_2 gas phase potential. We also note that the barrier to subsurface penetration is high for $\theta=90$ degrees, about 0.9 eV.

Figure 3b shows the PES for the end-on approach, $\theta=0$ degrees. There is an energy minimum for a geometry with one atom in the bridge position and the other atom between the first and second metal layer directly beneath the bridge site, but this is not stable with respect to the bottom of the H_2 gas phase potential. To reach this minimum a barrier of almost 2 eV has to be climbed.

Figures 3c and 3d show the PES's for $\theta=120$ and $\theta=60$ degrees, respectively. For positive values of the Z coordinate they are quite similar. Once the molecule has passed a small barrier of about 0.12 eV in the entrance channel the atoms can move freely towards a geometry with one atom above the surface and the other below. But the $\theta=60$ degrees PES develops a much more pronounced repulsive wall for negative values of Z than the $\theta=120$ degrees PES. This is due to what has already been discussed above. For the $\theta=120$ degrees approach one of the atoms ends up close to the hcp site; the other moves in the direction of a subsurface octahedral site and meets little resistance. The atom going subsurface in the $\theta=60$ degrees approach moves towards the tetrahedral subsurface site and feels the repulsion from the Pd atom in the second metal layer directly beneath the hcp site.

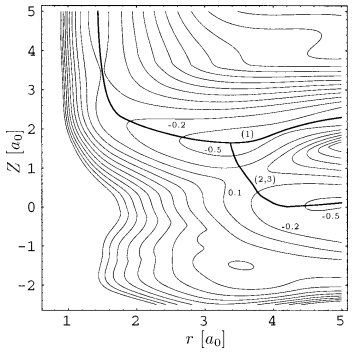

FIG. 4. The figure shows a contour plot of the PES resulting when the 3D PES has been minimized with respect to the angular variable. The numbers without the parentheses are in eV and give the value of the contour line that lies closest by. The energies are given relative to the bottom of the H_2 gas phase potential, and the contour spacing is 0.3 eV. Three reaction paths are also indicated in the plot and labeled by the numbers within the parentheses. The values of the angular coordinate along these reaction paths are given in Fig. 5a.

Figures 3e and 3f show the PES's for $\theta=150$ and $\theta=30$ degrees, respectively. Again they are quite similar for positive Z values. They both show a large barrier towards reaching a geometry with one atom above the surface and the other below. But now the effect of the position of the subsurface atom is much larger. For $\theta=150$ degrees the PES has a minimum with one atom close to the hcp site and the other close to the subsurface octahedral site which is stable by about 0.25 eV compared to the bottom of the H_2 gas phase potential. The minimum for $\theta=30$ degrees with one atom close to the fcc site and the other close to the tetrahedral subsurface site is not stable with respect to the bottom of the H_2 gas phase potential.

Figure 4 shows the PES resulting when the 3D PES has been minimized with respect to the angular variable. Also shown in the figure are the Z and r coordinates of three reaction paths. The values of the angular variable along these three reaction paths are given in Fig. 5a, and Fig. 5b shows how the adsorption/absorption energy (with respect to the bottom of the H_2 gas phase potential) varies along the reaction path coordinate, s. Reaction paths (1) and (2) represent minimum energy paths, whereas reaction path (3) is no minimum energy path. It is identical to (2) in the Z and r coordinates, but the angular variable along (3) takes the values $\theta_3=180-\theta_2$, with θ_2 being the value of the angular variable along (2). Reaction path (3) serves to show the large difference between the subsurface sites below the fcc and hcp sites. The figures clearly show that there are two end geometries that are stable with respect to the bottom of the H_2 gas phase potential. The first lies at the end of reaction path (1) shown in Figs. 4 and 5. Reaction path (1) has a local minimum for both hydrogen atoms on the surface, one close to the fcc site, the other close to the hcp site ($s\approx 4.5a_0$). This geometry can be reached by letting the hydrogen molecule

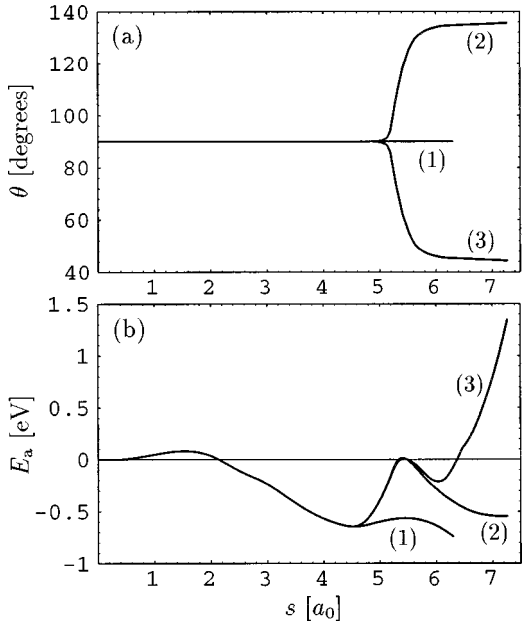

FIG. 5. Figure (a) shows the value of the angular variable (θ) along the three reaction paths discussed in the text and shown in Fig. 4, as a function of a reaction path coordinate (s). Figure (b) gives the molecule–surface interaction energies (E_a) along these reaction paths as a function of the same reaction path coordinate. The branching of the reaction paths in Fig. 4 occurs for $s \approx 4.5 a_0$.

approach the surface with its molecular axis parallel to the surface (θ=90 degrees) and passing a small barrier in the entrance channel of 0.09 eV. It is stable by about 0.65 eV as mentioned above. We also see from Fig. 5b that the global minimum along reaction path (1) is for a geometry where the two hydrogen atoms are shifted away from the threefold sites. As discussed in Ref. 18 this is due to the repulsion between the hydrogen atoms—two hydrogen atoms prefer to be further away from each other than the distance between neighboring fcc and hcp sites. The other stable geometry lies at the end of reaction path (2) and has one hydrogen atom in the hcp site and the other in the subsurface octahedral site. This geometry can be reached by approaching the surface with the molecular axis parallel to the surface (θ=90 degrees), passing the 0.09 eV barrier in the entrance channel and the surface adsorption minimum, and then rotating the molecule quite fast while increasing the distance between the hydrogen atoms and moving the molecule's center of mass closer to the surface. A second barrier (0.02 eV) has to be climbed to reach the final geometry, but this barrier is lower than the one in the entrance channel. The final geometry is stable by about 0.55 eV. Results for a third reaction path, reaction (3), are also given in Fig. 5. Since the final geometry is energetically unstable with respect to the bottom of H_2 gas phase potential it does not deserve to be called a reaction path, but it illustrates what has already been discussed above very clearly—a hydrogen atom penetrating the subsurface directly below a hcp site experiences strong repulsion from the closest Pd atom in the second metal layer.

It is important to note that the barrier to direct subsurface absorption is strongly dependent on the angle of the approaching hydrogen molecule. For the energetically more favorable angles the barrier to direct subsurface absorption is only about 0.02 eV (after the 0.09 eV barrier in the entrance channel has been passed). Other angles give large barriers. We also note that it is not only the part of the 3D PES with one or both hydrogen atoms subsurface that shows a strong dependence on the angular coordinate. The part of the PES describing geometries with both atoms above the surface also has a considerable angular dependence.

III. THE WAVE PACKET CALCULATIONS

The 3D Hamiltonian governing the motion of the hydrogen molecule is given by

$$\hat{H} = -\frac{1}{2M}\frac{\partial^2}{\partial Z^2} - \frac{1}{2\mu}\frac{\partial^2}{\partial r^2} - \frac{1}{2\mu r}\frac{\partial^2}{\partial \theta^2} + V(Z,r,\theta), \quad (2)$$

where the total and reduced mass are written as M and μ, respectively. According to the time-dependent close-coupling wave packet approach of Mowrey and Kouri[31,32] the wave function, $\Psi(Z,r,\theta,t)$, can at any time be expanded as

$$\Psi(Z,r,\theta,t) = \sum_{j=-N}^{N} \phi_j^{j_0}(Z,r,t)\frac{1}{\sqrt{2\pi}}\exp(ij\theta), \quad (3)$$

where j_0 labels the initial rotational state of the molecule and the Fourier expansion is truncated at N. This gives the close-coupling equations

$$i\frac{\partial}{\partial t}\phi_{j'}^{j_0}(Z,r,t) = \left[-\frac{1}{2M}\frac{\partial^2}{\partial Z^2} - \frac{1}{2\mu}\frac{\partial^2}{\partial r^2} + \frac{j'^2}{2\mu r}\right]\phi_{j'}^{j_0}(Z,r,t) + \sum_{j=-N}^{N} V_{j'j}(Z,r)\phi_j^{j_0}(Z,r,t), \quad (4)$$

with

$$V_{j'j}(Z,r) = \frac{1}{2\pi}\int_0^{2\pi} d\theta V(Z,r,\theta)\exp[i(j-j')\theta]. \quad (5)$$

The interaction potential, $V(Z,r,\theta)$, and the potential coupling matrix, $V_{j'j}(Z,r)$, will be discussed later. The initial wave function, $\Psi(Z,r,\theta,t_0)$, is given by inserting

$$\phi_j^{j_0}(Z,r,t_0) = \delta_{jj_0}\chi_{\nu_0 j_0}(r)\int dk_z b(k_z)\frac{1}{\sqrt{2\pi}}\exp(ik_z Z), \quad (6)$$

in Eq. (3), where $\chi_{\nu_0 j_0}(r)$ is a rovibrational eigenfunction of a hydrogen molecule rotating in a plane and labeled by the quantum numbers ν_0 and j_0, and $b(k_z)$ is the momentum distribution function for motion in Z given by

$$b(k_z) = \left(\frac{2\zeta^2}{\pi}\right)^{1/4}\exp[-(k_{z_0}-k_z)^2\zeta^2 + i(k_{z_0}-k_z)Z_0]. \quad (7)$$

The width of the momentum distribution function is determined by ζ, the average translational momentum and the center of the initial wave function are given by k_{z_0} and Z_0, respectively. Propagating the wave function in time is done

by acting with the time evolution operator, $e^{-i\hat{H}t}$, on the initial wave function according to the Chebyshev technique[33] as described in Refs. 31, 32, 34.

The expansion coefficients, $\phi_j^{j_0}(Z,r,t)$, in Eq. (3) are represented on 2D grids with equally spaced gridpoints covering the region $-6.0<Z<18.0a_0$ and $0.2<r<9.2a_0$ with 240 and 60 points in the Z and r directions, respectively. In the expansion of Eq. (3) we have used $N=48$. Due to the inversion symmetry of H_2 only even (odd) j-states have to be considered in the expansion of the wave function for j_0 even (odd). The action of the kinetic energy operators in Z and r on the wave function in Eq. (4) is found by the fast Fourier transform technique.[35,36] The 3D PES presented in the previous section has not been calculated outside the region $-2.5<Z<5.0a_0$ and $0.7<r<5.0a_0$, but we use the same technique as in Refs. 18, 19 to ensure we have an interaction potential defined on the whole grid. The H_2 gas phase potential, $V_{H_2}(r)$, is appended to the 3D PES in the following manner:

$$\begin{aligned}
&c_n(Z,r)=c_n'(Z,r), \quad Z\leqslant 5.0a_0, \quad n\in\{1,6\},\\
&c_1(Z,r)=f_{\text{switch}}(Z)c_1'(5.0a_0,r)+(1-f_{\text{switch}}(Z))\\
&\qquad\times V_{H_2}(r), \quad 5.0a_0<Z<6.75a_0,\\
&c_n(Z,r)=f_{\text{switch}}(Z)c_n'(5.0a_0,r), \quad 5.0a_0<Z<6.75a_0,\\
&\qquad n\in\{2,6\},\\
&c_1(Z,r)=V_{H_2}(r), \quad Z\geqslant 6.75a_0,\\
&c_n(Z,r)=0, \quad Z\geqslant 6.75a_0, \quad n\in\{2,6\},
\end{aligned} \tag{8}$$

with

$$f_{\text{switch}}(Z)=\frac{1}{2}+\frac{1}{2}\cos(\chi), \quad \chi=\frac{(Z-5.0a_0)\pi}{1.75a_0}. \tag{9}$$

For $Z<-2.0a_0$ the coefficients $c_n(Z,r)$ are set equal to their values along the line $Z=-2.0a_0$ and for $r>5.0a_0$ equal to their values along the line $r=5.0a_0$. The interaction potential in Eqs. (2) and (5) is then given by

$$\begin{aligned}
V(Z,r,\theta)=&c_1(Z,r)+c_2(Z,r)\cos(2\theta)+c_3(Z,r)\sin(2\theta)\\
&+c_4(Z,r)\cos(4\theta)+c_5(Z,r)\sin(4\theta)\\
&+c_6(Z,r)\cos(6\theta).
\end{aligned} \tag{10}$$

The potential coupling matrix, $V_{j'j}(Z,r)$, in Eqs. (4) and (5) can then easily be evaluated analytically and expressed in terms of the coefficients $c_n(Z,r)$. The coupling matrix is then seen to be very sparse. Combined with the fact that the kinetic energy operator in the angular coordinate is diagonal, as seen from Eq. (4), this leads to very favorable scaling with respect to the number of expansion functions. This is the reason for choosing to work with the time-dependent close-coupling wave packet approach of Mowrey and Kouri.[31,32]

To avoid artificial reflection from the boundaries of the grids quadratic optical potentials[37] have been used to absorb the wave packets in the regions $-6.0<Z<-2.0a_0$, $12.1<Z<18.0a_0$, and $5.0<r<9.2a_0$. In the Chebyshev expansion a time step of 100 a.u. (2.4 fs) has been used. This is short enough to avoid the Chebyshev expansion becoming unstable upon including optical potentials.[38] The projection operator formalism of Neuhauser and Baer[39] has been used to bring the initial wave packet in on a separate, one-dimensional grid, thus reducing the size of the grid in the Z direction.

To be able to distinguish the situation when one or both hydrogen atoms go subsurface from both staying on the surface, we use the flux formalism described in Refs. 18, 19, 38, 40. The energy resolved reaction probability is found from

$$P(k_z)=\frac{2\pi}{|k_z|}\text{Im}\int_S \mathbf{j}(k_z)\,d\mathbf{S}, \tag{11}$$

where $\mathbf{j}(k_z)$ is the energy resolved flux vector given by

$$\begin{aligned}
\mathbf{j}(k_z)=&\Psi^{+*}(k_z|Z,r,\theta)\frac{\partial\Psi^{+}(k_z|Z,r,\theta)}{\partial Z}\mathbf{e}_Z\\
&+\frac{M}{\mu}\Psi^{+*}(k_z|Z,r,\theta)\frac{\partial\Psi^{+}(k_z|Z,r,\theta)}{\partial r}\mathbf{e}_r\\
&+\frac{M}{\mu}\Psi^{+*}(k_z|Z,r,\theta)\frac{\partial\Psi^{+}(k_z|Z,r,\theta)}{\partial \theta}\mathbf{e}_\theta,
\end{aligned} \tag{12}$$

with $\mathbf{e}_Z$, $\mathbf{e}_r$, and $\mathbf{e}_\theta$ being the unit vectors in the Z, r, and θ directions, respectively. The stationary wave functions $\Psi^{+}(k_z|Z,r,\theta)$ and their derivatives are found by time to energy Fourier transforms as described in Refs. 18, 19, 34, 38, 40. From Fig. 2 we see that if Z lies under the surface described by

$$Z=\frac{1}{2}r|\cos(\theta)|, \quad r\in[0,r_{\text{flux}}], \quad \theta\in[0,2\pi), \tag{13}$$

one or both of the hydrogen atoms are beneath the surface plane. To use this curved surface in evaluating the surface integral in Eq. (11) we would have to calculate the full flux vector in Eq. (12). If we on the other hand consider the surface combined of two flat surfaces,

$$Z=0, \quad r\in[0,r_{\text{flux}}], \quad \theta\in[0,2\pi), \tag{14}$$

and

$$r=r_{\text{flux}}, \quad Z\in\left[0,\frac{1}{2}r_{\text{flux}}|\cos(\theta)|\right], \quad \theta\in[0,2\pi), \tag{15}$$

only one of the three terms in Eq. (12) would need to be calculated for each surface. Since the two approaches are equivalent we choose the less computationally demanding one. Thus the energy resolved direct subsurface absorption probability is found by integrating the appropriate part of the flux vector over the surface defined by Eqs. (14) and (15). The probability for both atoms ending up on the surface is found by evaluating the surface integral in Eq. (11) over the surface,

$$r=r_{\text{flux}}, \quad Z\in\left(\frac{1}{2}r_{\text{flux}}|\cos(\theta)|,Z_{\text{flux}}\right], \quad \theta\in[0,2\pi), \tag{16}$$

where $r_{\text{flux}}=5.0a_0$ and $Z_{\text{flux}}=18.0a_0$. The total reaction probability is found by adding the surface and subsurface reaction probabilities.

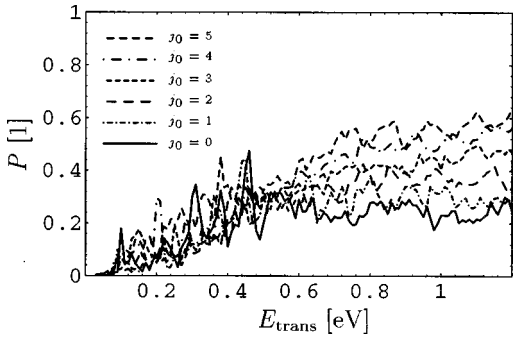

FIG. 6. The probability (P) for one or both hydrogen atoms going directly subsurface as a function of the collision energy (E_{trans}), for different initial rotational states (j_0). The hydrogen molecule is initially in its ground vibrational state.

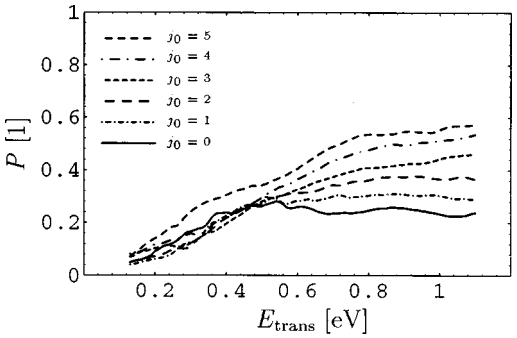

FIG. 7. The figure shows the convolution of the curves in Fig. 6, where the convolution given in Eqs. (17) and (18) has been used. P labels the probability for one or both hydrogen atoms going directly subsurface, E_{trans} the collision energy, and j_0 the initial rotational states.

IV. RESULTS

The probabilities for one or both hydrogen atoms going directly subsurface for different initial molecular rotational states are shown in Fig. 6. The hydrogen molecule is initially in its ground vibrational state. We see that hydrogen penetrates directly into the subsurface region already at incident kinetic energies of about 0.05 eV, and at an energy of 0.2 eV a substantial part of the hydrogen goes directly subsurface. The results from our 3D model therefore support the experimental evidence presented by Gdowski, Stulen, and Felter[6] for hydrogen going directly subsurface without equilibrating in the chemisorption well on the surface.

In Ref. 18 the quantum dynamical wave packet calculations on the 2D DFT PES did not give any support for direct subsurface absorption at low incident kinetic energies. In the present study the dynamical wave packet calculations on the new 3D DFT PES do show substantial subsurface penetration at low energies. What would happen if we would include all six molecular degrees of freedom in our calculations? Would we still find support for direct subsurface absorption? As will be suggested below, and also indicated in Ref. 19, dynamical steering[41] (by forces the molecule experiences as it travels along the PES which tend to make the molecule follow minimum energy paths towards the final geometries) plays an important role in the low energy regime of direct subsurface absorption of hydrogen on Pd(111). Our present study has indicated a favorable reaction path on the PES leading to hydrogen ending up below the surface plane. Dong and Hafner[23] do not consider the possibility for direct subsurface absorption, but they give results for three reaction paths not considered here, where the hydrogen atoms end up in the threefold chemisorption sites on the surface. If extended to the subsurface region they would probably show similar energetics as the path considered in this study, although the subsurface penetration would occur for a larger H–H separation. Thus there will be a number of reaction paths present on a six-dimensional (6D) PES including all molecular degrees of freedom leading to hydrogen ending up below the surface plane and dynamical steering will guide hydrogen along these favorable paths to the subsurface region. We therefore believe that a 6D treatment of the H_2+Pd(111) system would also display direct subsurface absorption at low incident kinetic energies.

In Ref. 19 it was shown that Pd surface motion introduced important qualitative and quantitative effects in the direct subsurface absorption when two of the hydrogen molecular degrees of freedom were treated. Treating more molecular degrees of freedom together with Pd surface motion might open up more subsurface channels, again suggesting that theoretical calculations would agree with the experimental results of Gdowski, Stulen, and Felter[6] in that they would show direct subsurface absorption.

The subsurface probabilities show a lot of structure, as also seen in the 2D calculations in Ref. 18. The peaks that are seen are likely to be due to resonances. Resonances that can affect a reaction are entrance channel resonances (the reactant is trapped in a well, and its vibration against the barrier enhances the reaction) and transition state resonances (which arise from quantization of the motions perpendicular to the reaction path at the transition state). Entrance channel resonances often give rise to the peak structure seen also in the present results (see for example Ref. 42). Transition state resonances are usually manifest from sudden rises in the reaction probability, followed by a leveling off (see for example Ref. 43). Because this staircase behavior is not seen in our results, it is less likely that transition state resonances cause the structure seen. It is more likely that the structure is due to trapping in front of the barrier to subsurface penetration (see also Fig. 3a). However, a further analysis of the resonances was not made in the present paper. Rather, to be able to see the trends in Fig. 6 more clearly we have convoluted the the curves by using the convolution

$$P_{\mathrm{conv}}(E_{\mathrm{trans}}) = \int dE \;\; f(E;E_{\mathrm{trans}})P(E), \tag{17}$$

where

$$f(E;E_{\mathrm{trans}}) = \begin{cases} \dfrac{1}{2\Delta E}, & E_{\mathrm{trans}} - \Delta E < E < E_{\mathrm{trans}} + \Delta E, \\ 0, & \text{otherwise}, \end{cases} \tag{18}$$

with $\Delta E = 0.1$ eV. The results are given in Fig. 7. For $j_0 = 0$ and $j_0 = 1$ the probabilities show an increase with in-

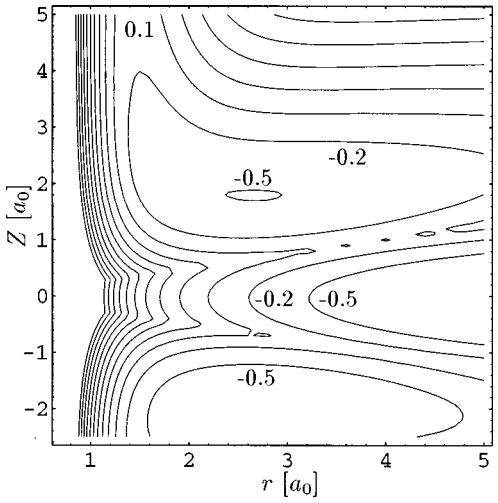

FIG. 8. Contour plot of the LEPS PES for an angle of $\theta=120$ degrees used by Munn and Clary (Ref. 17). See Fig. 3c for a comparison. The numbers within the contour plot are in eV and give the value of the contour line that lies closest by. The number 0.1 pertains to the two closest contour lines. The energies are given relative to the bottom of the H_2 gas phase potential, and the contour spacing is 0.3 eV.

creasing incident kinetic energies until about 0.5 eV, then a small decrease and flattening out for higher energies. For $j_0=2$, $j_0=3$, $j_0=4$, and $j_0=5$ there is a continuous increase in subsurface penetration with increasing energies. A difference between the low (<0.5 eV) and high (>0.5 eV) collision energy regime is that in the low energy regime the direct subsurface absorption first decreases with increasing j_0 and then increases again with further increasing j_0, whereas in the high energy regime the direct subsurface absorption simply increases with increasing j_0. The low energy behavior is similar to what is seen in experiments for the total reaction probability.[44,45] A slow incoming hydrogen molecule in the ground rotational state can be oriented around a favorable geometry for penetrating the subsurface region. Increasing the rotational energy will make it more difficult to orient or keep the molecule oriented around a favorable geometry. But increasing the rotational or the incident kinetic energy also makes a larger part of the PES accessible to the molecule. The competition between these two effects can explain the results seen in Fig. 7.

Our results show both qualitative and quantitative differences from the results of Munn and Clary[17] for a hydrogen molecule in its rotational and vibrational ground state. This is not due to the reduced-dimensionality approximations they used to perform their 3D calculations, but rather the PES they employed in the calculations. In Fig. 8 we show a contour plot of the LEPS PES they used for an angle of $\theta=120$ degrees. Comparing this with the DFT PES presented in Fig. 3c we see that the 3D LEPS PES suffers from only being parametrized for one value of the angle ($\theta=90$ degrees) and not the full range of angles. Thus, as the authors themselves pointed out, the 3D LEPS PES they used does not model direct subsurface absorption very well. But their study did nevertheless show the importance of including an angular degree of freedom in the PES and also indicated that including an angular degree of freedom would open up the possibility of hydrogen going directly subsurface even at low incident kinetic energies.

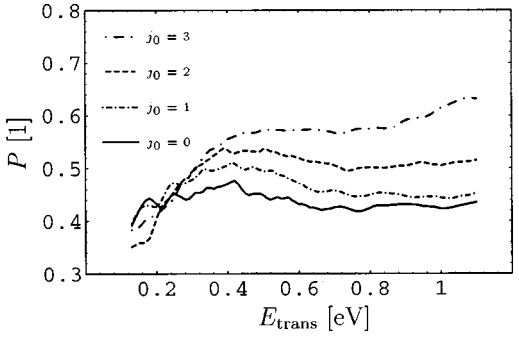

FIG. 9. The probability (P) for one or both hydrogen atoms going directly subsurface as a function of the collision energy (E_{trans}), for different initial rotational states (j_0). The hydrogen molecule is initially in its first vibrationally excited state. The convolution of Eqs. (17) and (18) has been used.

In the 2D study of Ref. 18 it was shown that vibrationally exciting the hydrogen molecule was very efficient in promoting direct subsurface absorption. Figure 9 shows the direct subsurface absorption probabilities for a hydrogen molecule in its first vibrationally excited state and different initial molecular rotational states. Comparing these results to those in Fig. 7 we see that vibrationally exciting the hydrogen molecule is also in this 3D treatment very efficient in promoting direct subsurface absorption. We also note that Figs. 7 and 9 show a similar trend with respect to dynamical steering—both show that in the low energy regime the direct subsurface absorption first decreases with increasing j_0 and then increases again with further increasing j_0, whereas in the high energy regime the direct subsurface absorption simply increases with increasing j_0.

The total reaction probabilities are shown in Fig. 10 and we see that the probabilities tend to zero when the incident kinetic energies approach zero. This seems to disagree with the experimental results in Refs. 44–47 which indicate a nonzero sticking coefficient for the low energies. In Ref. 46 the results are interpreted to indicate that there is no barrier in the entrance channel, whereas the authors in Ref. 47 claim their results point to a barrier of about 50 meV. The reason

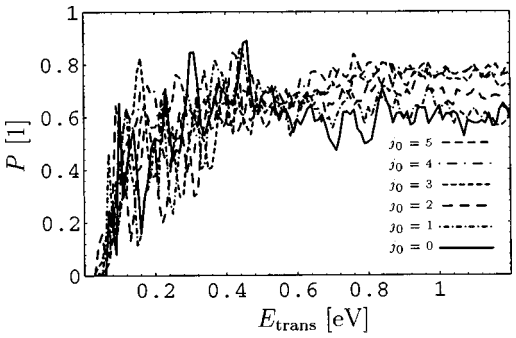

FIG. 10. The total reaction probability (P), i.e., the probability for the hydrogen molecule not being reflected back to the gas phase, as a function of the collision energy (E_{trans}), for different initial rotational states (j_0). The hydrogen molecule is initially in its ground vibrational state.

for their assumption of a barrier is that the sticking coefficient initially decreases with increasing incident energies—the hydrogen molecule is thought to be trapped in a molecular precursor state as a step in the dissociation process, which would favor the slow incoming molecules. In Ref. 44 decreasing dynamical steering is thought to be the reason for the initial decrease in the sticking coefficient and no barrier is inferred. Thus the experiments do not seem to answer the question of whether there are barrierless reaction paths or not to H_2 dissociation on Pd(111). The question of whether molecular precursor states play a role in the dissociation or not seems also to be left unanswered by experiments.

In the DFT GGA calculations by Dong, Kresse, and Hafner[24] five different paths to dissociation were considered and all showed a barrier in the entrance channel. In a more recent study by Dong and Hafner[23] the same five paths, plus two additional paths, to dissociation were considered. Four paths were reported to be nonactivated. Two of these paths had earlier been said to be activated. Both studies agree with the results that the path considered in Section II is slightly activated. But as seen from Fig. 3a and 3b in Ref. 19 the barrier in the entrance channel almost disappears when including Pd surface motion. Thus it is not completely clear whether DFT at the GGA level predicts barrierless reaction paths to dissociation or not for the H_2+Pd(111) system. Further our 3D PES shows no molecular precursor state, in agreement with the results of Dong, Kresse, and Hafner[24] and Dong and Hafner.[23] Their results do, however, indicate the presence of molecular precursor states for other reaction paths.

There are thus three possible explanations for the disagreement between our total reaction probabilities tending to zero and the nonzero sticking coefficient seen in experiments. If trapping into molecular precursor states is an important step in the dissociation process and this is the reason for the high sticking coefficients at the low energies, we would not be able to model this with our present 3D PES since this PES does not show any molecular precursor wells. Another explanation could be that DFT at the GGA level wrongly predicts a barrier in the entrance channel for the reaction path considered in this study—the true PES might have no barrier to dissociation and quantum mechanical wave packet calculations on such a PES would yield nonzero reaction probabilities even at the low energies.[41] A third possible explanation is that, as indicated by the results of Dong and Hafner,[23] the 6D DFT GGA PES do have barrierless reaction paths for other approach geometries than the one considered here, or, as indicated in Ref. 19, Pd surface motion might remove the barrier in the entrance channel. A model study including such barrierless reaction paths in the DFT GGA PES would again give nonzero reaction probabilities for the low energies when performing quantum mechanical wave packet calculations.

The influence of molecular rotation on the total reaction probability is shown in Figs. 10 and 11. The figures show similar trends as seen for direct subsurface absorption—in the low energy regime the total reaction probability first decreases with increasing j_0 and then increases again with further increasing j_0. This is in qualitative agreement with the

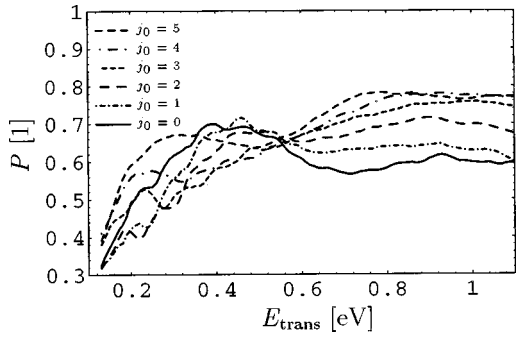

FIG. 11. The figure shows the convolution of the curves in Fig. 10 using Eqs. (17) and (18). P labels the total reaction probability, E_{trans} the collision energy, and j_0 the initial rotational states.

experimental results of Refs. 44, 45 which indicated efficient steering for the rotational ground and lower rotationally excited states.

Finally, our planar rotor model of the hydrogen molecule allows for both positive and negative values of the initial rotational quantum number j_0 as seen from Eqs. (3) and (4). This reflects the possibility for clockwise and counterclockwise rotation within the plane. In this study we have been focusing on the influence of including an angular degree of freedom for the H_2 molecule on a qualitative level, and the results for negative j_0 show all the same qualitative trends as for the positive j_0. However, there are some points worth commenting on. In Fig. 12 we show results for direct subsurface absorption for molecules initially in the $j_0=1$ and $j_0=-1$ states. Since we believe dynamical steering is very important in the low energy energy regime, it should not make much difference whether the molecule rotates clockwise or counter-clockwise initially, and this is also what we see in Fig. 12. But in the high energy regime the $j_0=1$ molecules exhibit higher direct subsurface absorption probabilities than the $j_0=-1$ molecules. This can be understood

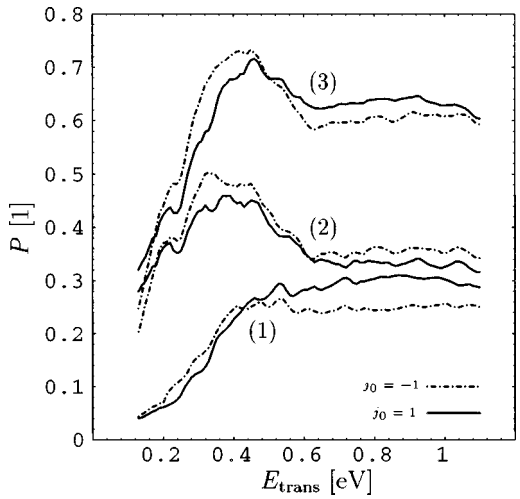

FIG. 12. The probability (P) for one or both hydrogen atoms going directly subsurface (1), the probability for dissociative chemisorption (2), and their sum, i.e., the probability for the hydrogen molecule not being reflected back to the gas phase (3) as a function of the collision energy (E_{trans}), for $j_0=1$ and $j_0=-1$. The hydrogen molecule is initially in its ground vibrational state and the convolution given in Eqs. (17) and (18) has been used.

from Figs. 3, 4, and 5 and the discussion in Sec. II. The $j_0 = 1$ molecules rotate in a direction of increasing θ and this rotational direction leads towards a favorable absorption geometry, whereas the rotational direction of the $j_0 = -1$ molecules lead towards an unfavorable absorption geometry. These trends are seen for $|j_0| = 1$ through $|j_0| = 5$ (results not shown here), with the additional feature that the difference in the high energy regime becomes smaller with increasing $|j_0|$. A tentative explanation for the latter effect is that the rotational motion for high, positive j_0 is too fast compared to the motion in Z and r to lead towards a favorable absorption geometry.

The effects described in the previous paragraph can perhaps be observed experimentally. With the use of a magnetic field perpendicular to the plane of rotation as defined in the present work, ''top-spin'' and ''back-spin'' states which are very similar to the $j_0 = 1$ and $j_0 = -1$ planar rotor states discussed here, can be made using state-selection techniques pioneered in the late sixties.[48] Such experiments would yield a difference between the $j_0 = 1$ and $j_0 = -1$ direct subsurface absorption probabilities if we assume that (i) direct subsurface penetration mainly takes place with the hydrogen molecule's center of mass at the bridge sites and that (ii) bridge site 1 is much more reactive for subsurface penetration than bridge sites 2 and 3 (of Fig. 1). The second assumption seems reasonable in that for a molecule aligned parallel to the plane of incidence as defined in the present work, reaction at bridge sites 2 and 3 would not follow a reaction path with the atoms ending up in or passing through the threefold hollow sites and therefore be reduced. Furthermore, with a molecule aligned parallel to the plane of incidence as described above, the only other impact site which would allow the hydrogen atoms to reach the subsurface region is the top site. But the barrier to subsurface penetration would then be found at larger H–H separation, making direct subsurface penetration less likely, thus supporting the first assumption above. To measure the effects the experiments should also distinguish between dissociative chemisorption and direct subsurface absorption, which may be to hard to accomplish. However, as Fig. 12, shows the rotational direction also affects the dissociative chemisorption and total reaction probabilities. A measurement of this effect would be interesting even if only for the total reaction probability. So far, experiments[49–51] and theoretical calculations[41,52–54] have only addressed the influence of molecular orientation with respect to the surface, looking at ''cartwheel'' ($m_j = 0$) and ''helicopter'' ($m_j = \pm j$) states, where the quantization axis is perpendicular to the surface. It should be interesting also to explore the effect of the rotational direction, i.e., the sign of m_j, where m_j is defined with respect to a quantization direction parallel to the surface. We should also note that the alignment parallel to the plane for $m_j = \pm j$ states improves with increasing j, suggesting that the effect might be easier to verify experimentally for high j.

V. CONCLUSIONS

Using density functional theory (DFT) within the generalized gradient approximation (GGA) a three-dimensional (3D) potential energy surface (PES) including an angular degree of freedom was calculated for the H_2+Pd(111) system. The 3D PES shows an entrance channel barrier (≈ 0.09 eV) to both dissociative chemisorption and direct subsurface absorption, but after this barrier is crossed direct subsurface absorption can proceed almost without a barrier (≈ 0.02 eV). The 3D PES is also seen to be strongly dependent on the angular degree of freedom with the barrier for subsurface penetration ranging from the said 0.02 eV to almost 2 eV.

Quantum mechanical wave packet calculations employing the 3D PES showed hydrogen going directly subsurface even at low incident kinetic energies. This is in good agreement with the experimental evidence presented by Gdowski, Stulen, and Felter[6] that hydrogen can absorb directly subsurface without first equilibrating in the chemisorption well on the surface.

We also saw that in the high incident energy regime (>0.5 eV) direct subsurface absorption increased with increasing j_0. In the low incident energy regime (<0.5 eV) the strong dependence on the angular degree of freedom in the 3D PES led to rotation inhibiting direct subsurface absorption at low j_0 and promoting it at high j_0. The low energy results showed the same qualitative trend as seen in experiments for the behavior of the sticking coefficients,[44,45] and this can be explained by the competition between dynamical steering[41] at low rotational energies and accessibility of larger parts of the PES at high rotational energies.

For the lowest incident kinetic energies the total reaction probabilities found in our calculations tended to zero, whereas experiments[44–47] show nonzero sticking coefficients in this regime. This discrepancy could possibly be caused by molecular precursor states not modeled in our 3D DFT GGA PES being responsible for nonzero sticking, DFT at the GGA level wrongly predicting barriers in the entrance channel, or our model not including barrierless reaction paths that might exist on the full-dimensional DFT GGA PES, where full-dimensional refers to both hydrogen molecular degrees of freedom and Pd surface degrees of freedom.

The effect of the rotational direction on reaction probabilities has until now not been studied. Our calculations showed small quantitative differences between results for positive and negative j_0 and we therefore suggest further work in this direction, both experimental and theoretical.

ACKNOWLEDGMENTS

We are grateful to Professor S. Stolte for useful discussions on state-selection techniques and O. M. Løvvik for critical reading of the manuscript and suggesting improvements. The calculations reported here have been carried out under a grant of computer time by the Dutch National Computing Facilities Foundation (NCF). R.A.O. is financed by the Norwegian Research Council. G.J.K. acknowledges financial support by the Royal Netherlands Academy of Arts and Sciences (KNAW).

[1] W. Eberhardt, F. Greuter, and E. W. Plummer, Phys. Rev. Lett. **46**, 1085 (1981).
[2] W. Eberhardt, S. G. Louie, and E. W. Plummer, Phys. Rev. B **28**, 465 (1983).

[3] T. E. Felter, S. M. Foiles, M. S. Daw, and R. H. Stulen, Surf. Sci. Lett. **171**, L379 (1986).
[4] G. D. Kubiak and R. H. Stulen, J. Vac. Sci. Technol. A **4**, 1427 (1986).
[5] G. E. Gdowski, T. E. Felter, and R. H. Stulen, Surf. Sci. Lett. **181**, L147 (1987).
[6] G. E. Gdowski, R. H. Stulen, and T. E. Felter, J. Vac. Sci. Technol. A **5**, 1103 (1987).
[7] T. E. Felter, E. C. Sowa, and M. A. van Hove, Phys. Rev. B **40**, 891 (1989).
[8] C. T. Chan and S. G. Louie, Phys. Rev. B **30**, 4153 (1984).
[9] M. S. Daw and S. M. Foiles, Phys. Rev. B **35**, 2128 (1987).
[10] D. L. Lynch, S. W. Rick, M. A. Gomez, B. W. Spath, J. D. Doll, and L. R. Pratt, J. Chem. Phys. **97**, 5177 (1992).
[11] S. W. Rick, D. L. Lynch, and J. D. Doll, J. Chem. Phys. **99**, 8183 (1993).
[12] J. Rogan, M. Lagos, and I. K. Schuller, Surf. Sci. Lett. **318**, L1165 (1994).
[13] R. Löber, Ph.D. thesis, Humboldt-University of Berlin, 1995.
[14] O. M. Løvvik and R. A. Olsen, J. Chem. Phys. **104**, 4330 (1996).
[15] J. F. Paul and P. Sautet, Phys. Rev. B **53**, 8015 (1996).
[16] R. Löber and D. Hennig, Phys. Rev. B **55**, 4761 (1997).
[17] N. S. Munn and D. C. Clary, Chem. Phys. Lett. **266**, 437 (1997).
[18] R. A. Olsen, P. H. T. Philipsen, E. J. Baerends, G. J. Kroes, and O. M. Løvvik, J. Chem. Phys. **106**, 9286 (1997).
[19] R. A. Olsen, G. J. Kroes, O. M. Løvvik, and E. J. Baerends, J. Chem. Phys. **107**, 10652 (1997).
[20] G. te Velde, Ph.D. thesis, Vrije Universiteit, Amsterdam, 1990.
[21] G. te Velde and E. J. Baerends, Phys. Rev. B **44**, 7888 (1991).
[22] http://tc.chem.vu.nl/SCM/Doc/BANDUG/BANDUG.html.
[23] W. Dong and J. Hafner, Phys. Rev. B **56**, 15396 (1997).
[24] W. Dong, G. Kresse, and J. Hafner, J. Mol. Catal. A: Chem. **119**, 69 (1997).
[25] P. Hohenberg and W. Kohn, Phys. Rev. **136**, B864 (1964).
[26] W. Kohn and L. J. Sham, Phys. Rev. **140**, A1133 (1965).
[27] J. E. Worsham, Jr., M. K. Wilkinson, and C. G. Shull, J. Phys. Chem. Solids **3**, 303 (1957).
[28] K. Sköld and G. Nelin, J. Phys. Chem. Solids **28**, 2369 (1967).
[29] J. M. Rowe, J. J. Rush, L. A. de Graf, and G. A. Ferguson, Phys. Rev. Lett. **29**, 1250 (1972).
[30] G. Nelin and K. Sköld, J. Phys. Chem. Solids **36**, 1175 (1975).
[31] R. C. Mowrey and D. J. Kouri, Chem. Phys. Lett. **119**, 285 (1985).
[32] R. C. Mowrey and D. J. Kouri, J. Chem. Phys. **84**, 6466 (1986).
[33] H. Tal-Ezer and R. Kosloff, J. Chem. Phys. **81**, 3967 (1984).
[34] R. C. Mowrey and G. J. Kroes, J. Chem. Phys. **103**, 1216 (1995).
[35] D. Kosloff and R. Kosloff, J. Comput. Phys. **52**, 35 (1983).
[36] M. D. Feit, J. A. Fleck, Jr., and A. Steiger, J. Comput. Phys. **47**, 412 (1982).
[37] Á. Vibók and G. G. Balint-Kurti, J. Phys. Chem. **96**, 8712 (1992).
[38] D. Neuhauser, M. Baer, R. S. Judson, and D. J. Kouri, Comput. Phys. Commun. **63**, 460 (1991).
[39] D. Neuhauser and M. Baer, J. Chem. Phys. **91**, 4651 (1989).
[40] D. H. Zhang and J. Z. H. Zhang, J. Chem. Phys. **101**, 1146 (1994).
[41] A. Gross, S. Wilke, and M. Scheffler, Phys. Rev. Lett. **75**, 2718 (1995).
[42] G. J. Kroes, G. Wiesenekker, E. J. Baerends, R. C. Mowrey, and D. Neuhauser, J. Chem. Phys. **105**, 5979 (1996).
[43] A. D. Kinnersley, G. R. Darling, S. Holloway, and B. Hammer, Surf. Sci. **364**, 219 (1996).
[44] M. Beutl, M. Riedler, and K. D. Rendulic, Chem. Phys. Lett. **247**, 249 (1995).
[45] M. Gostein and G. O. Sitz, J. Chem. Phys. **106**, 7378 (1997).
[46] T. Engel and H. Kuipers, Surf. Sci. **90**, 162 (1979).
[47] C. Resch, H. F. Berger, K. D. Rendulic, and E. Bertel, Surf. Sci. Lett. **316**, L1105 (1994).
[48] H. Moerkerken, M. Prior, and J. Reuss, Physica **50**, 499 (1970).
[49] D. Wetzig, R. Dopheide, M. Rutkowski, R. David, and H. Zacharias, Phys. Rev. Lett. **76**, 463 (1996).
[50] S. J. Gulding, A. M. Wodtke, H. Hou, C. T. Rettner, H. A. Michelsen, and D. J. Auerbach, J. Chem. Phys. **105**, 9702 (1996).
[51] H. Hou, S. J. Gulding, C. T. Rettner, A. M. Wodtke, and D. J. Auerbach, Science **277**, 80 (1997).
[52] G. R. Darling and S. Holloway, J. Chem. Phys. **101**, 3268 (1994).
[53] J. Dai and J. Z. H. Zhang, J. Chem. Phys. **102**, 6280 (1995).
[54] R. C. Mowrey, G. J. Kroes, G. Wiesenekker, and E. J. Baerends, J. Chem. Phys. **106**, 4248 (1997).